Dynamic modelling of the thermal response enhanced by sloshing in marine LNG fuel tanks

Erlend Liavåg Grotle[a,*], Vilmar Æsøy[a]

[a]*Department of Ocean Operations and Civil Engineering, Norwegian University of Science and Technology (NTNU), NO-6009 Ålesund, Norway*

Abstract

This paper investigates the thermal response in marine liquefied natural gas (LNG) fuel tanks by experiments and modelling. The aim of this work is to develop phenomenological models that can predict the rapid pressure loss experienced onboard LNG fuelled vessels. Experiments have been conducted using water. A horizontally aligned tank made of steel has the same geometry as a LNG fuel tank, but at model scale. The tests are performed by supplying heat to evaporate water that is led through a closed loop from the bottom to the top passing a heating element. A lumped dynamic model is developed that can be tuned by adjusting few parameters. Uniform conditions are assumed in each phase. The model can provide useful insight and be combined with other submodels to perform system simulations. Good correspondence with the experimental data is found after tuning heat transfer coefficients, air content in the gas and the average temperatures. After validating the model, it is used to predict the necessary heat supplied to the pressure build-up unit (PBU) to maintain the tank pressure. A simple relation between the measured pressure and the PBU heat capacity is presented.

Keywords: Sloshing, dynamic models, experiments, heat transfer, LNG fuel tanks

1. Introduction

Natural gas as a fuel has proven beneficial for the environment [1]. The number of ships fuelled with liquefied natural gas (LNG) has increased the recent years, and operational experience has shown that ensuring reliable operation is still challenging. One of the challenges are related to the thermodynamic response inside the LNG fuel tank, influenced by sloshing. Sloshing can be characterized as the motion of liquids in containers or vessels [2]. Traditionally, concerns with sloshing are damages due to impact forces. Sloshing may also alter the ship stability, but is also used to enhance the ship stability with roll-stabilizer tanks. The rapid pressure drop in the LNG fuel tanks is related to the motion, filling depth and the temperature of the bunkered LNG. The consequence of such a pressure drop is shutdown of the gas engines, as the system pressure may drop below a minimum required for reliable operation [3]. The potential pressure

*Corresponding author
Email address: erlend.l.grotle@ntnu.no (Erlend Liavåg Grotle)

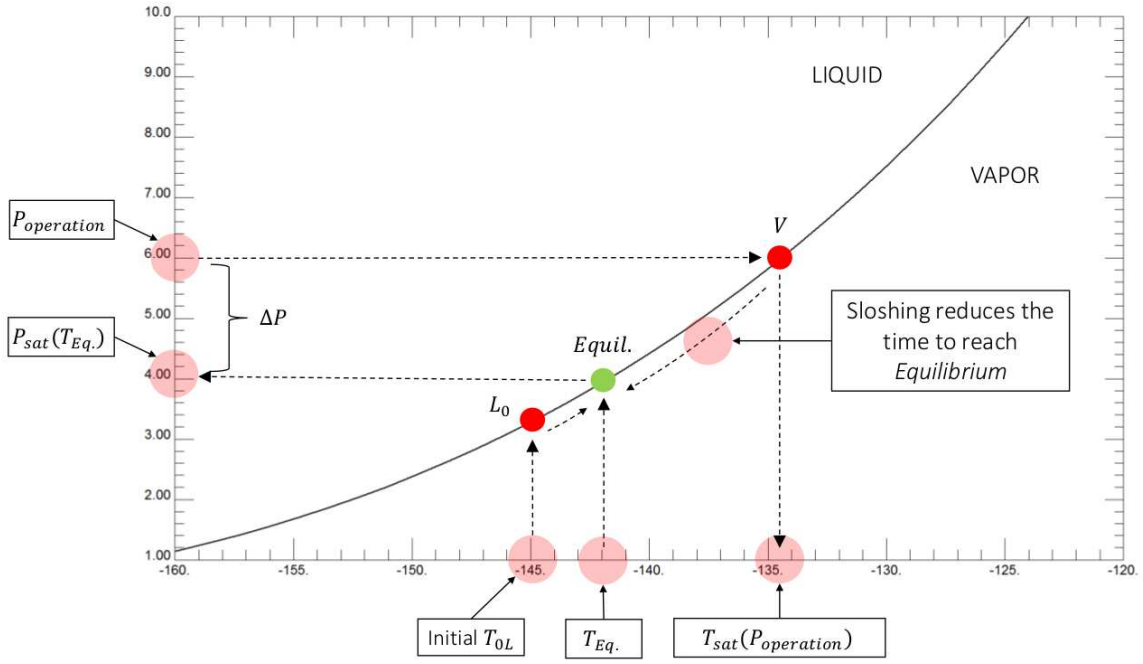

Figure 1: Co-existence curve for methane. The P-T data was generated using REFPROP v9.1 [4].

drop in a tank with a single component fluid can be explained by considering the co-existence curve for methane (Fig. 1).

The potential pressure drop corresponds to the maximum possible temperature difference between the liquid bulk and the saturation temperature of the operational pressure. The operating pressure corresponds to a T_{sat}, which is higher than the bunkered liquid temperature. If it is assumed that the liquid temperature remains the same, the potential final pressure corresponds to this temperature. The liquid temperature is also increasing, depending on its mass. The superheated gas counteracts the subcooled liquid, but the larger liquid mass makes it dominating the process.

Moran *et al.* [5] investigated the thermodynamic response due to sloshing in a liquid hydrogen tank by performing experiments with varying excitation frequency. The pressure collapse magnitude was recorded, as well as the temperature at different locations. Unstable sloshing conditions with an excitation close to the first mode natural frequency was found to have the greatest impact on the pressure drop, while stable sloshing were found to have minor effect.

Lacapere *et al.* [6] compared experimental tests and numerical simulations to investigate the influence of interface heat and mass transfer on the pressure evolution due to sloshing using both liquefied nitrogen (LN_2) and liquefied oxygen (LOx). Comparison between the numerical simulations and experiments shows that the de-stratification in the liquid is responsible for the large pressure drop.

Arndt [7] presented experiments in his PhD thesis, and found that the presence of non-condensible gas reduces the condensation and increases the evaporation. This indicates that condensation is responsible for

the majority of the energy transfer.

Ludwig *et al.* [8] conducted several experiments using liquefied nitrogen (LN_2) in a vacuum-insulated upright cylindrical tank. All of the experiments were conducted with one translational motion amplitude, except in the last case. The excitation frequency was varied in proximity to the first mode natural frequency, representing regimes that cover the range of stable planar wave motion to swirl waves. A Nusselt number were introduced that correlates with a sloshing Reynolds number based on wave amplitude and frequency.

Sloshing in a horizontally aligned pressure vessel were investigated by Grotle et al. [9] using LN_2 as test medium. The influence of frequency and initial pressure is presented in the paper. It was found that the pressure drop rate depends on the frequency, and the most significant occurs close to the first mode natural frequency. The total pressure drop is influenced by the initial pressure, but to reach the potentially minimum, a certain sloshing intensity is required.

From the mentioned studies there are strong evidence that direct energy exchange takes place between the liquid and the gas. This is also the hypothesis in this project. Direct-contact heat transfer can be beneficial with the large contact area between the phases, and the thermal resistance of a solid wall is also excluded [10]. There are several industrial processes where direct-contact heat transfer are applied. One example is fluid mixing by an axial jet which is a method to reduce tank pressure of a two-phase system in which the fluid is thermally stratified. This is done to prevent pressure rise due to external heating in a cryogenic tank [11], [12]. Mahood *et al.* [13] made a theoretical prediction of the transient characteristics of a two-phase, two-component direct-contact condenser. Joseph *et al.* [14] studied the effect of insulation thickness on the pressure evolution in a cryogenic tank. The tank model is divided into an ullage gas volume and a liquid volume. The pressurization is investigated using the ideal gas law with a compressibility factor. The same modelling principle is used in our model, assuming that the latent heat must balance the total sensible heat, and that the sensible heat consist mainly of convection.

Modelling of thermodynamic systems by the bond graph technique is inspired by Karnopp [15], Moksnes [16], Pedersen [17]. and Thoma [18].

2. Objectives

A lumped dynamic model may be useful when several subsystems are joined together to perform system simulations, because the models are computational efficient. In the case of LNG fuelled ships, the fuel system itself consist of several units, including the tank, pressure build-up unit (PBU), main evaporator, gas recovery unit (GRU) and the gas engines with propulsion- and control system. Although our modelling approach is fairly simple, it can provide useful insight by combining it with experimental results.

In this paper, a two-compartment dynamic model is developed to represent the thermal response due to sloshing. The main focus is the mechanisms that cause the rapid pressure loss experienced on-board LNG

fuelled ships. Experiments have been conducted with a model scaled LNG fuel tank. Liquid water and vapour is used as test medium. A discussion about the similarity between methane and water is presented in the last part. To study the sloshing regimes, tests with a transparent tank of similar size are presented as well. The thermodynamic model is developed using the bond graph technique, which is a graphical method to combine several ordinary differential equations to a system of equations that can be solved numerically. The aim is to tune the model according to experiments with only a limited number of parameters. Only a few tests are presented here, but they represent different sloshing regimes. This is done on purpose to better emphasize the effect of sloshing on the pressure drop.

As to our knowledge, there are no similar studies presented with such a modelling technique to represent direct-contact heat- and mass transfer enhanced by sloshing. No similar tests involving the thermal response in a horizontally aligned pressure vessel can be found as far as to the authors knowledge. Few general sloshing studies considering semi-elliptic pressure vessels exist, and so the preliminary investigation of the transparent tank is a contribution as well.

The results show that our dynamic model represent the thermodynamic response quite accurately by tuning few parameters. The greatest uncertainty in the model is the spatial distribution of internal energy. It is found that the assumption of convection in the bulk as the driving mechanisms for condensation is too rough. The relation between the condensation mass flow and the bulk convection is too tightly coupled considering uniform conditions in each phase. This is because we can not separate the area from the heat transfer coefficients, and with lack of a proper formulation of the condensation mass flow rate. A simple way to predict the PBU power need from the measured pressure is presented in the last part of the paper.

3. Model description

3.1. Mass and energy balance

By considering the whole tank as a system, the total energy balance can be written as the sum of internal, kinetic and potential energy.

$$dU + dE_k + dE_p = \delta Q - \delta W, \tag{1}$$

where U is the total internal energy of the tank, E_k and E_p are kinetic and potential energy respectively. Q is heat and W is work transferred to the system. We consider only heat supply to the PBU (Fig. 2). The work term consist of pressure-volume work and external work. We assume that all the work input corresponds to the sum of the change in kinetic and potential energy. These terms then vanish. This is the same as assuming that there is no change in internal energy due to dissipation of kinetic energy.

The tank system is divided into two compartments that exchange internal energy, one for liquid and one for gas, as shown in Fig. 2. Heat is also transferred to the PBU. The energy balance for the total tank system

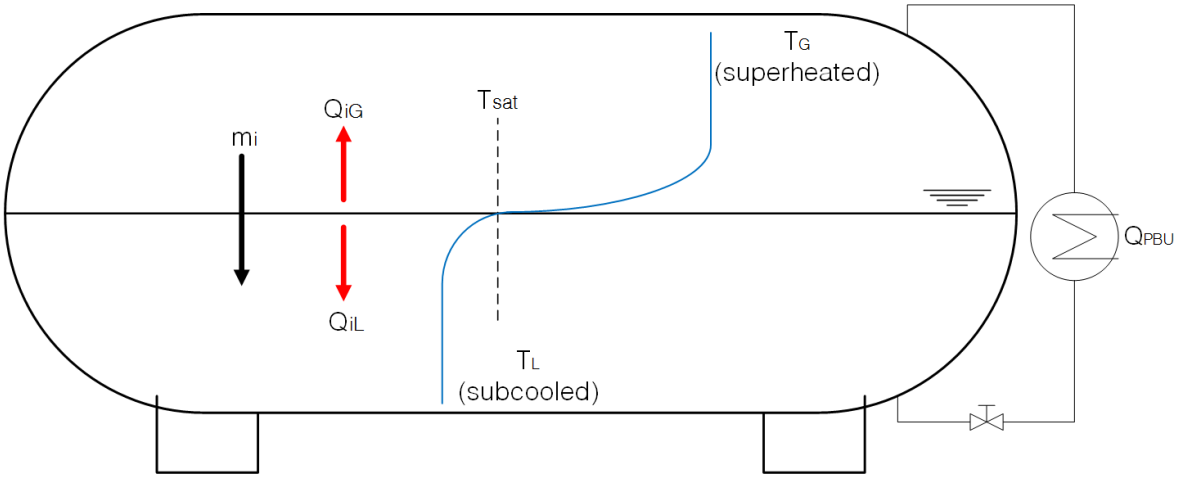

Figure 2: Model description.

then reads

$$dU_L + dU_G = \dot{Q}_{PBU}, \tag{2}$$

where the subscripts, L and G mean liquid and gas respectively. Our assumption of no heat losses is acceptable since the heat transfer between the phases is much greater during the period of sloshing. As explained in the previous sections, the purpose of the PBU in the fuel system is to maintain the tank pressure. The heating element is used in the experiments compensate the for the pressure during sloshing.

For the mass, we have the following condition

$$dm_L + dm_G = 0. \tag{3}$$

As the total tank volume is constant, the volume is also conserved, so that

$$dV_L + dV_G = 0. \tag{4}$$

The liquid density is kept constant in the model. This means that the gas density can be solved for when both the volume and mass in each phase are used as state variables.

In addition to this, we have the energy balance for each of the phases, where the internal energy is given as:

$$\frac{dU_G}{dt} = \dot{m}_G u_g + \dot{Q}_{iG} - p\frac{dV_G}{dt} + \dot{Q}_{PBU}, \tag{5}$$

$$\frac{dU_L}{dt} = \dot{m}_L u_f + \dot{Q}_{iL} - p\frac{dV_L}{dt}. \tag{6}$$

Here $\dot{Q}_{iG}$ and $\dot{Q}_{iL}$ are sensible heat fluxes in the gas- and liquid bulk. $\dot{m}_G$ is the evaporation mass flux equal to dm_G/dt. u_g and u_f are the specific saturation internal energy for gas and liquid respectively.

$\dot{Q}_{PBU}$ is the heat supplied to the heating element, and is defined as

$$\dot{Q}_{PBU} = \dot{m}_{PBU} \cdot \left[h_{fg} + c_{v,L} \left(T_{sat} - T_L \right) \right], \tag{7}$$

where h_{fg} is the specific enthalpy of formation and $c_{v,L}$ is the specific heat capacity of the liquid.

Summing Eq. 5 and Eq. 6 and subtracting the result from Eq. 2 it can be shown that

$$u_{fg} \dot{m}_L = \dot{Q}_{iG} + \dot{Q}_{iL}. \tag{8}$$

This is the interface condition which shows that the sensible heat is balanced by latent heat. If there is no mass exchange, the heat flux must be the same on each side of the interface. Positive heat flux is defined as positive into a control volume. By considering that the heat flux is always directed towards decreasing temperature, the value of the gas side sensible heat would be negative, while the liquid side positive (see Fig. 2). $\dot{m}_L$ is the condensation mass flux. Increasing the superheated gas temperature would then reduce $\dot{m}_L$, while reducing liquid temperature would increase $\dot{m}_L$.

The specific internal energy is $u = U/m$ and a simple relation between the specific internal energy and temperature is used,

$$u_G - u_g = c_{v,G} \left(T_G - T_{sat} \right), \tag{9}$$

$$u_L - u_f = c_{v,L} \left(T_L - T_{sat} \right). \tag{10}$$

$T_{sat} = T(P_v)$ is the saturation temperature which is assumed to be the temperature at the interface, and a function of the vapour pressure, P_v.

The assumption of uniform conditions means that a mass-averaged temperature must be considered to ensure that the energy balance is fulfilled. This may easily result in errors as the spatial distribution is not entirely known from the experiments. As far as possible, the experimental measurements are used to find a mass-averaged value. In some of the cases, the information is still not enough to know how the temperature is distributed spatially. In this work we approximate the values by weighting the energy content by a factor. This is adjusted until the energy balance is fulfilled. This must be done after the other parameters are determined as will be explained in the following. The resulting average temperature are then compared to the measured values. Working with averaged values like this is probably the largest uncertainty of our model.

The sensible heat on each side of the interface, $\dot{Q}_{iG}$ and $\dot{Q}_{iL}$ can be defined according to Newtons law of cooling

$$\dot{Q}_{iG} = -h_{iG} \cdot A_i \left(T_G - T_{sat} \right), \tag{11}$$

$$\dot{Q}_{iL} = -h_{iL} \cdot A_i \left(T_L - T_{sat}\right). \tag{12}$$

h_{iG} and h_{iL} are the heat transfer coefficients for the gas and liquid side of the interface respectively. A_i is the interface area. Each of them can not be known by tuning the model, but the product. $h_i \cdot A_i$ can be found by comparing the simulated temperature and pressure with the experimental results. The tuning of these parameters only changes the speed, not the final state.

The liquid temperature has significant influence on the pressure due to the large mass. The gas side heat transfer coefficient has only a minor impact on the pressure, but influences the proximity of the gas temperature to the saturation temperature. The experimental saturation temperature is found from the pressure. The low influence of the gas side heat transfer coefficient on the pressure makes it possible to assume saturation conditions in the gas without changing the final state much. This is the same as assuming a very large heat transfer coefficient.

The pressure can be related to the gas temperature and density by the ideal gas law,

$$P = \rho_G R T_G, \tag{13}$$

where R is the individual gas constant, equal to R_u/M and R_u is the universal gas constant, ρ_G is the gas density and M the mole weight.

Air is present in the gas pocket during the tests and its contribution to pressure must be accounted for. The mass of dry air is unknown, but can be found by assuming that the saturation temperature must correspond to the equilibrium temperature of liquid and gas. The saturation temperature is a function of the vapour pressure. The change in the fluid properties, like the specific heat capacity is also taken into account.

The concept of specific humidity can be used [19]. Introducing the ideal gas law, we got:

$$\omega = \frac{m_v}{m_a} = \frac{M_v P_v V / R_u T}{M_a P_a V / R_u T} = \frac{M_v P_v}{M_a P_a}, \tag{14}$$

where we have introduced the partial pressure of water vapour ("v") and air ("a"), as well as the respective mole masses, M_v and M_a, with the ratio approximately equal to $M_v/M_a = 0.622$. The total pressure, P consist of the sum of these partial pressures, such that

$$P_v = P \cdot \left(\frac{0.622}{\omega} + 1\right)^{-1}. \tag{15}$$

In this way, the correct saturation temperature can be found from the vapour partial pressure.

3.2. Implementation of the model using bond graphs

The bond graph method provides a simple graphical method to solve a set of ordinary differential equations. A lumped model is only varying in time, and the state variables are integrated numerically using

20-sim [20]. The resulting bond graph is shown in Fig. 3. Each C-element represent accumulation of mass and internal energy in each phase. The resultant flux (right-hand side of Eq. 5 and Eq. 6) is integrated to give the new effort variables. The two MSf-elements at the right are pressure-volume work, which is minor in this case. The R-element (”Ev”) represent the sensible heat flux on each side of the interface. The sum is equal to the latent heat, and the mass flux is calculated inside the same R-element. The mass- and energy fluxes are calculated in the beginning of each time step based on the difference of the effort variables which in this case is the temperature. All the saturation properties are found by interpolation in thermodynamic tables. The PBU-power of the heating element is supplied with the Sf-element (”Heat”). The mass and energy flow through the heating element is calculated in side the R-element (”Element”).

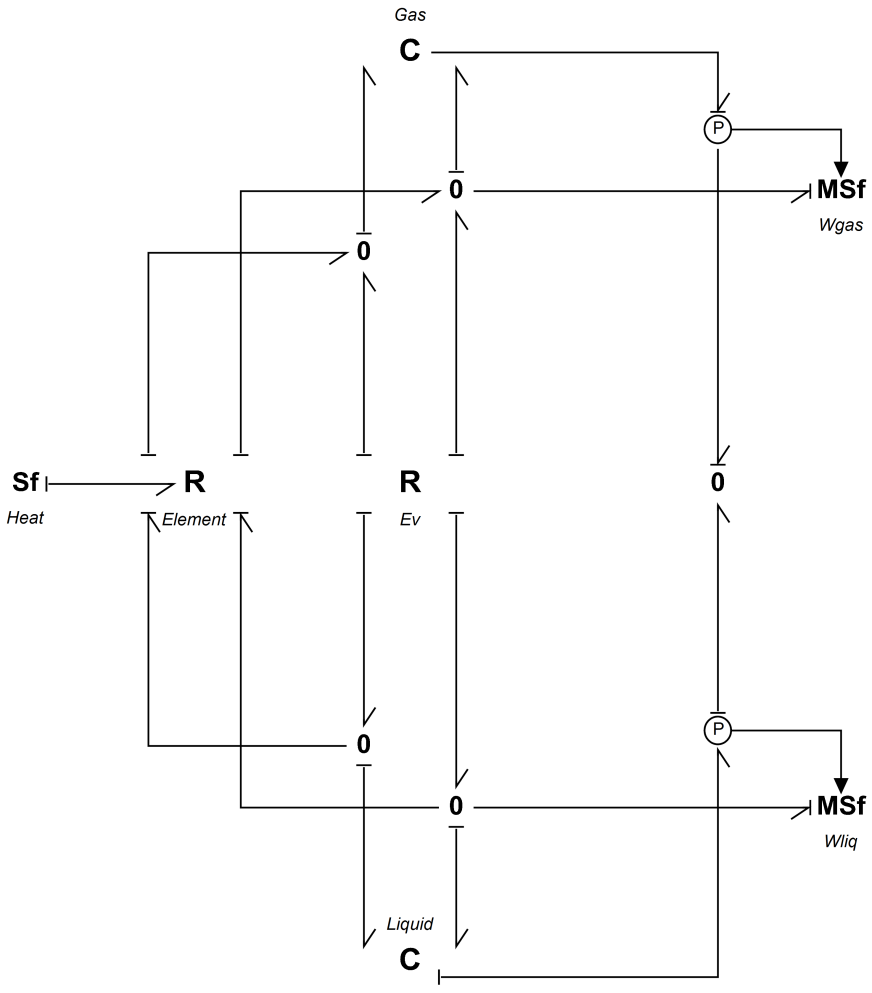

Figure 3: Bond graph model.

4. Experimental set-up

4.1. Thermal tank test

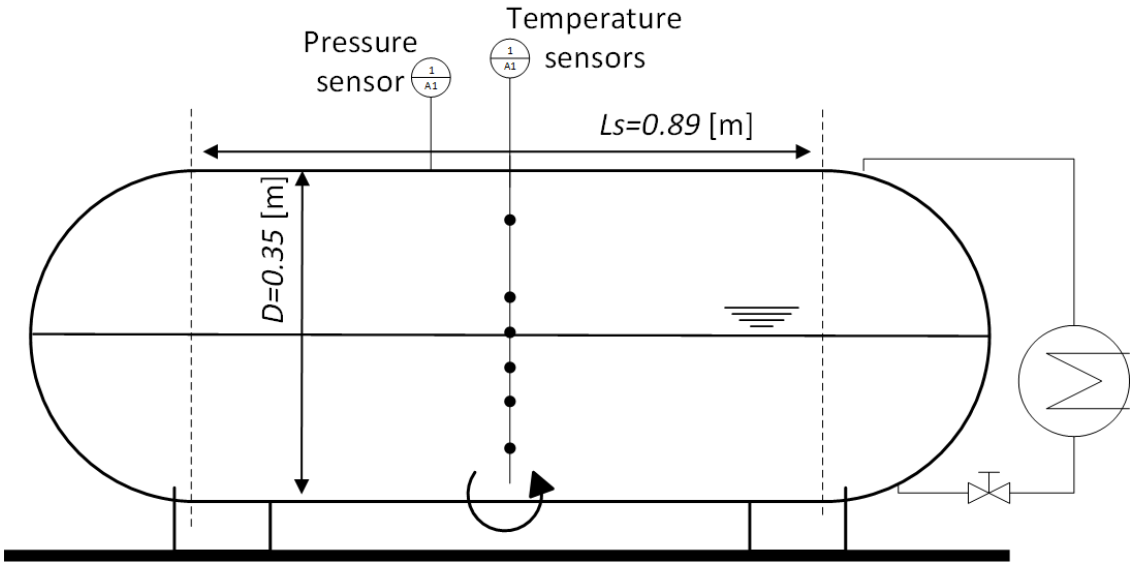

Figure 4: Thermal tank and the instrumentation.

Table 1: Specifications of instrumentation and devices.

Device	Type	Range	Accuracy
Temperature sensor	Thermocouple type T	-270-370 [°C]	±1.0 [°C]
Pressure sensor	P8AP	0-20 [bar]	0.3 %
Heating element	Høiax	0-1460 (max. 3000) [W]	-
Voltage supply	Philips 2422 530 05401	0-260 [V]	-
Electro-motor	MAC800-D2	750 [W] @ 3000 RPM	±0.5 % (speed)

The experimental work presented in this paper consists of tests performed with an insulated cylindrical pressure tank. The set-up is shown in Fig. 4. It consist of instrumentation like pressure sensor and several thermocouples placed vertically in the middle of the tank. The instruments and their specification are given in Table. 1. At the right side on Fig. 4, a variant of a unit PBU has been installed. A heating element is heated by using an external voltage supply. The mean water depth in the tank is 50 % in all tests. The heater is placed lower than the mean depth, and the flow of water and vapour is driven by hydrostatic pressure differences. The relationship between mass flux and power supply is measured in advance to know the amount of vapour.

The test procedure consist of initial heating of the liquid from approximately 15-20 degC to 120 degC. This ensures that the ΔT does not get too large. The heater is adjusted to the maximum power possible. For these tests, the power has been limited to 1460 [W]. In the beginning, the tank is left open to remove air. However, removing air from the system can be challenging, so it is expected that the presence of air must

Table 2: Sloshing test conditions. h/D is the mean height to diameter relationship, L_s $[m]$ is the length of the cylindrical section, f $[Hz]$ is the excitation frequency and $f/f_{1,0}$ is the frequency divided by the first mode natural frequency calculated for a rectangular tank with the same length as L_s. t_s $[s]$ is the length of the sloshing time.

Case No.	h/D	h/L_s	f $[Hz]$	$f/f_{1,0}$	t_s	Description
0	0.50	0.19	0.13	0.200	30	Flat surface
1	0.50	0.19	0.29	0.427	70	Small deformation
2	0.50	0.19	0.40	0.495	51	Oscillating waves
3	0.50	0.19	0.57	0.840	30	Jet formed

be accounted for. To build up the system temperature we switch between pressurisation with the heater and sloshing. The heat is then mixed more efficiently inside the tank.

When the system is ready for the sloshing tests, the pressure is increased to the desired value. The heater is turned off and the electro-motor starts with a specified frequency and number of periods.

4.2. Investigation of sloshing regimes

The thermal tank is not transparent. To study sloshing inside these tanks, a pre-study is also performed where a transparent tank of similar size and form is moved on a platform. Existing studies on horizontally aligned cylindrical tanks are limited, and the natural frequencies with these type of tank heads are unknown. Studies have been performed by the authors, but the results are not yet published.

A characteristic feature of the sloshing in these tanks is the jet that forms due to the spherical tank heads, as seen Fig. 5a. When the wave that builds up at the side wall hits the roof, the circular form lead the liquid in return with high speed. There is less impact against the roof compared to a square corner like in rectangular tanks. The jet goes approximately half way back in return before it hits the liquid surface with an inclined angle. The form and speed depends on filling and frequency. The frequency range is narrower for the lower fillings with a motion frequency closer to primary resonance. With fillings $h/D \geq 0.5$ like studied here, the jet is present in a broader frequency range.

The chosen sloshing parameters used in this preliminary study are given in Table 2. The same motion amplitude, filling and frequency were used to study the thermal response. The motion amplitude is kept constant and equal to 3 degrees in all tests. Several more experiments have been performed by the authors, but the listed conditions are chosen specifically to validate the dynamic model.

In case number 0 the frequency is very low. The free surface remains flat and the wetting of the walls is only due to the inclination angle. There is no break-up of the liquid-gas surface.

In the second case small waves are present, but the surface is not broken.

The third case is performed with a motion closer to the first mode natural frequency. Several waves are oscillating rapidly, like shown in Fig. 5b. The surface does not break, but steep standing waves sometimes result in some splashing.

Case 3 is at resonance so the sloshing is severe. The jet seen in Fig. 5a is present during the whole sloshing event.

(a) The jet formed due to the spherical heads (case number 3).

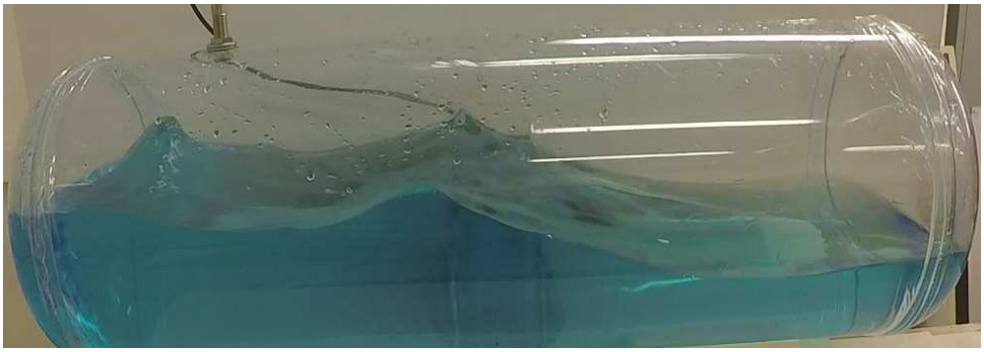

(b) Oscillating surface without breaking (case number 2).

Figure 5: Sloshing cases.

5. Results

5.1. Comparison of the pressure drop

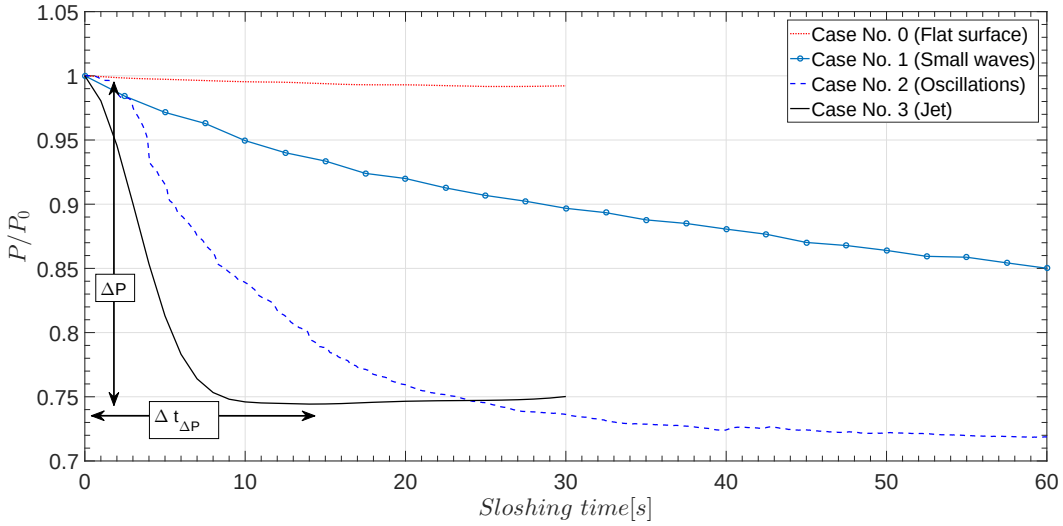

Figure 6: Measured pressure drop and its dependency on the motion frequency. P_0 is the maximum pressure before sloshing starts.

The resulting pressure evolution for the different cases is shown in Fig. 6. The sloshing starts at time 0 seconds in all cases. Although the number of sloshing time vary from case to case, only the first 60 seconds are shown in the figure. The heating element is turned off throughout the sloshing tests presented in this section.

It is clear that the most severe sloshing results in the most significant pressure drop. The pressure decreases 25 % in approximately 10 seconds in case number 3. Case 0 has almost unchanged pressure drop, while the pressure in case number 1 has not reached a minimum value after 60 seconds. The reason for the lower pressure in case number 2 is the lower air content in the gas. The results indicate that the pressure drop rate is large due to the large area of the broken free surface. The results also indicate that pressure is influenced by oscillating waves where the free surface area is significantly less than in case number 3. The local condensation takes place due to the large area and depends on hold up time and the size of the liquid drops and gas bubbles [12]. The condensation close to the interface between the gas and liquid rely on transport of energy between the interface and liquid bulk.

5.2. Validation of the model

Comparison of pressure and temperature is shown in Fig. 7 - Fig. 9. The time $t = 0$ $[s]$ is a few seconds after the actual start of the motion. This is because the product $h_{iL} \cdot A_i$ represent an average value during the sloshing time, and the start is not representative for this average. The agreement is good considering that

only a single parameter is tuned to represent sloshing intensity. The experimental temperatures in the figures are from the lower- and uppermost sensors in the liquid and gas. A mean value is found by interpolating between the saturation temperature and the bottom and top temperature. An equilibrium temperature is reached in case number 2 and 3. The time to reach this condition is much longer in case number 2 than in 3. The pressure in case 1 has not reached its minimum value when the sloshing stops. Case 0 is not included in the figure.

It can be seen from the measurements that the raise of the liquid temperature occur at a later time when the largest decrease in pressure already has taken place. It happens earlier in case 3 compared to case 2. This is due to the time it takes before the energy is mixed out from the interface to the bottom. Still, the pressure has almost reached a minimum value before the bottom temperature is affected. The pressure is sensitive to local condensation rates. For large fillings the liquid temperature is not influenced before a certain time of bulk mixing. As the condensation rate in the model is directly related to the bulk convection, and the spatial variation is unknown, the liquid temperature will increase differently than in the experiments. The condensation rates are not predicted correctly, but the tuned value gives the resulting pressure evolution. It must be noted that significant amount of gas is condensed in case number 2 before the liquid temperature at the bottom increases. Much less break-up of the surface is found in case number 2 than 3, and so a much less condensation rate is expected.

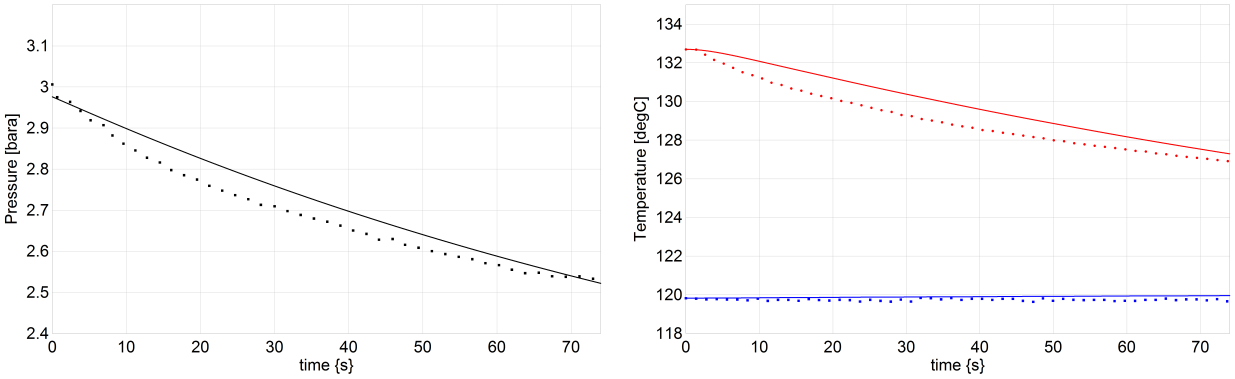

Figure 7: Pressure (left) and temperature (right) from **case 1** (Small waves) comparing experiments and simulations.

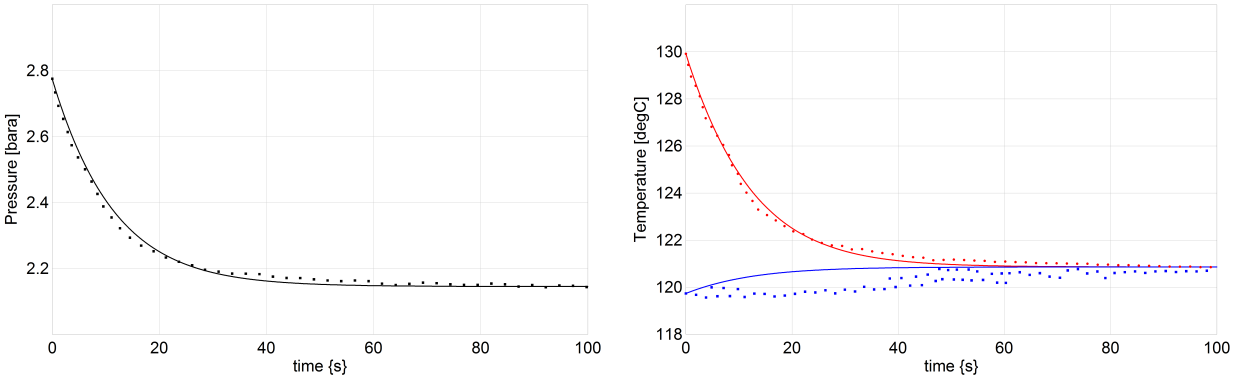

Figure 8: Pressure (left) and temperature (right) from **case 2** (Oscillations) comparing experiments and simulations.

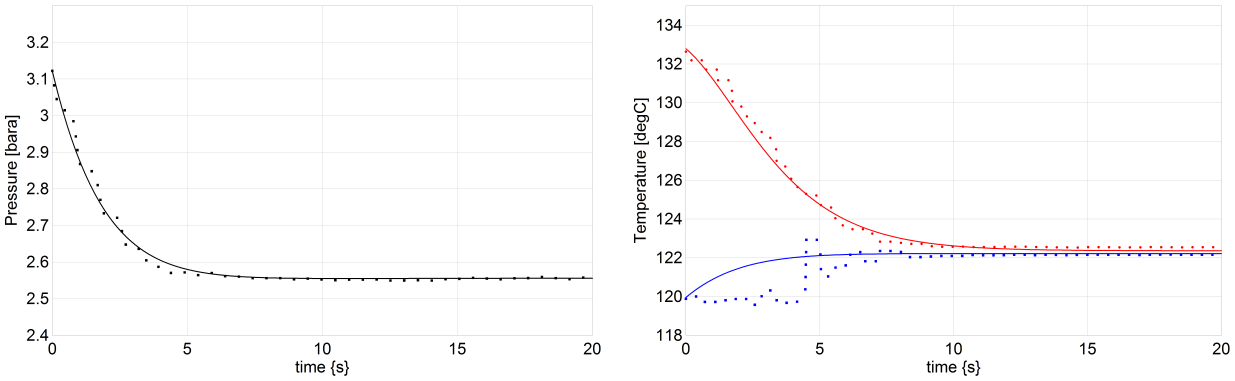

Figure 9: Pressure (left) and temperature (right) from **case 3** (Jet) comparing experiments and simulations.

Table 3: Results found from simulations and experiments. $m_{0,air}/m_{0,tot}$ is the initial mass fraction of air in the gas, $-\Delta P$ [bar] is the total pressure drop, P_{max} [bar] is the maximum absolute pressure before sloshing, $\Delta t_{\Delta P} \cdot f$ is the number of motion cycles to reach the minimum pressure, $h_{iL} \cdot A_i$ and $h_{iG} \cdot A_i$ $[W/m^2 \cdot K] \cdot [m^2]$ are the heat transfer coefficients times the interface area and $\Delta m_{cond}/\Delta m_{0,vap}$ is the total condensed mass fraction of the initial vapour mass during $\Delta t_{\Delta P}$.

Case No.	$\frac{m_{0,air}}{m_{0,gas}}$	$-\Delta P$ $[bar]$	P_{max} $[bar]$	$\Delta t_{\Delta P} \cdot f$	$h_{iL} \cdot A_i$	$h_{iG} \cdot A_i$	$\frac{\Delta m_{cond}}{m_{0,vap}}$
0	0.470	0.037	4.0254	N/A	9	50	0.02
1	0.030	0.453	3.0213	N/A	35	40	0.15
2	0.075	0.642	3.0086	40	330	170	0.23
3	0.240	0.569	3.1221	6	2500	50	0.21

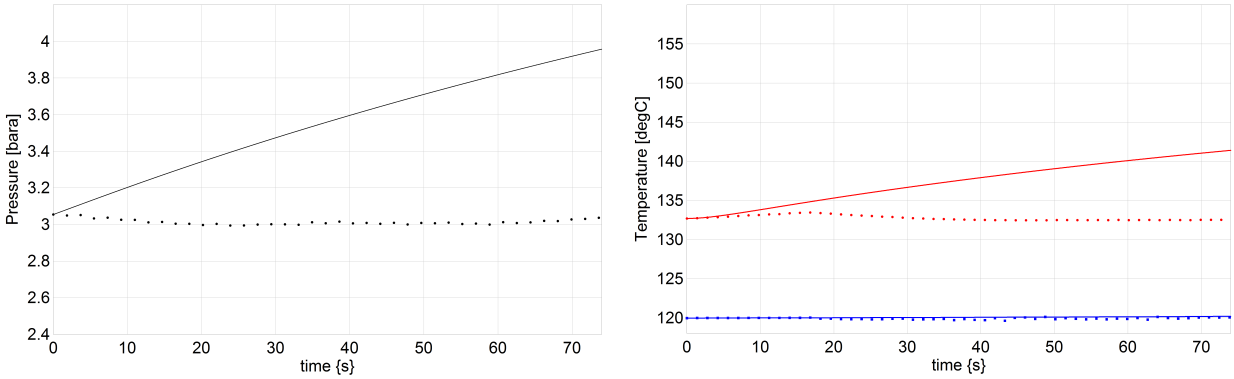

Figure 10: Pressure (left) and temperature (right) from case 1 with heat compensation and same tuning as in Fig. 7.

Tuned parameters and the results for all cases are shown in Table 3. Some differences between the initial values exist, like the pressure and the air content. The lower air content in case number 2 results in even lower pressure. It is also seen that more than 20 % of the initial vapour mass is condensed in case number 2 and 3, which results in a equilibrium condition. It can be seen from the table that the interface area is not separated from the heat transfer coefficient, as the interface area is unknown. An alternative way may be to predict the area using CFD methods, but this would hardly be accurate in case number 3. Its worth mentioning that the undisturbed interface area is 0.3557 m^2.

5.3. Prediction of heat compensation

The purpose of the PBU is to control the pressure when the liquid level is reduced. The same principle is used in land-based facilities. The power needed to compensate for the rapid pressure loss due to sloshing is a relevant matter. The PBU must deliver the same energy that corresponds to the condensation of the gas. The reduction in gas density has the largest influence on the pressure drop, and so the PBU must deliver the same amount of mass that is condensed.

The theoretical prediction of the mass flow for a given input power on the heating element can be calculated by Eq. 7. Experiments have been conducted to relate the power input, assumed to be $\dot{Q}_{PBU}$, to the mass flow of vapour. The results indicate that the mass flow is approximately 90 % of the theoretical value. Some external heat losses are expected. The relation between power and mass flow shows almost a linear trend.

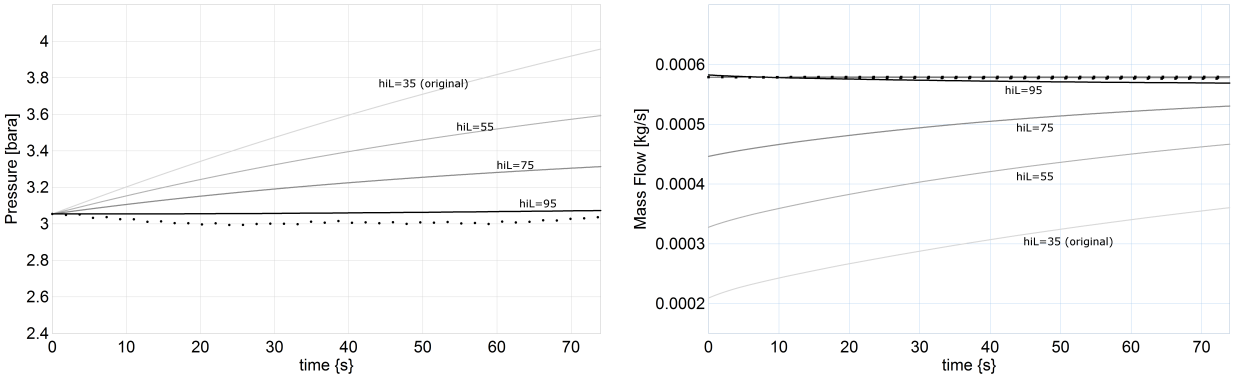

Figure 11: Pressure (left) and temperature (right) from case 1 with compensation and *increased* condensation rate relative to the initial settings in Fig. 10.

Case number 1 was found to have low enough frequency for the heating element to compensate for the pressure loss. The motion parameters are given in Table 2. The result is shown in Fig. 10. It can be seen that the pressure and temperature is over-predicted when the heating element is included in the simulations. The reason is probably the increased condensation rate when the gas is pressurized. In our model, this must accounted for by changing h_{iL}. By increasing this parameter slightly, we see that the mass flow of condensation approach the mass flow of the heating element (Fig. 11). Tuning of the heat transfer coefficient should be unnecessary in the case of pressurization. This is a consequence of the definition of the mass flow rate in our model.

The mass transfer at the interface due to condensation can be related directly to the pressure drop by differentiating Eq. 13 and assuming no change in the gas volume,

$$\frac{dm_L}{dt} = -\frac{m_G}{P} \cdot \frac{dP}{dt} + \frac{m_G}{T_G} \cdot \frac{dT_G}{dt}. \tag{16}$$

The change in temperature has minor effect on the pressure loss, and the rightmost term may be excluded. The power needed by the PBU is then the mass flux found from the pressure drop rate multiplied by the specific enthalpy of formation,

$$\dot{Q}_{PBU} = \frac{dm_L}{dt} \cdot h_{fg} \approx -\frac{m_G}{P} \cdot \frac{dP}{dt} \cdot h_{fg}. \tag{17}$$

We apply this to the measured pressure from case 1-3 by calculating the pressure drop rate numerically. The result is given in Fig. 12.

The calculated PBU power, $\overline{\dot{Q}}_{PBU}$ averaged over a sloshing cycle is given in Table 4. The power in case 1 varies in all of the 5 cycles shown. The sloshing is less intense, so the pressure drop is distributed over a longer period of time. In case 2 and 3, the pressure curve is steeper in the beginning and worst in case 3. The only case where a difference with and without compensation was found, is in case 1, as presented earlier in this section. The power supply to the element is limited to 1461 [W] in all of these tests. The reason is

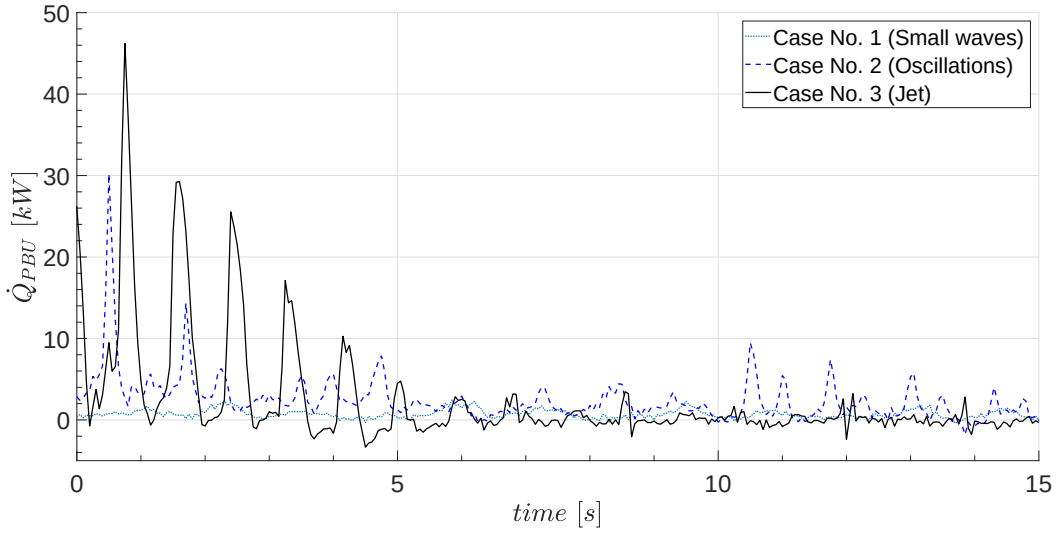

Figure 12: PBU power need estimated from the measured pressure.

Table 4: Predicted PBU power needed to compensate for the pressure drop is averaged the first 5 sloshing cycles.

Sloshing cycle no.:	1	2	3	4	5
		$\overline{\dot{Q}}_{PBU}$ [kW]			
Case 1:	0.976	0.711	0.845	0.638	0.599
Case 2:	3.808	2.676	2.107	2.346	1.506
Case 3:	11.486	7.235	1.731	0.373	0.279

limitations in the equipment. The theory predicts somewhat less power needed for compensation, equal to 980 [W] in case 1. Averaging over an even smaller part of the first cycle result in even larger power need.

6. Scaling and similarity analysis

Water has been used as a substitute for natural gas at model scale. The aim of the paper is not to find a substitute to LNG, but rather to investigate the phenomenon of sloshing enhanced mixing and pressure drop. This is why water is considered a good option. However, if results should be applicable to full scale there would need to be some scaling involved. A full scale tank may be as long as 30 metres, with a diameter of 5 metre. A prerequisite to perform model tests is to ensure geometrical similarity. For this tank type, the length-to-diameter, L/D must be the same. The tank heads and length of cylindrical section must have the same ratios. The non-dimensional filling (filling-to-length), h/L must be the same as well.

Scaling that considers fluid properties as well as compressible flow is not that easy to perform. Criteria for scaling of LNG sloshing was presented in Bass et al. [21]. In general, Froude analysis is sufficient if incompressible scaling is considered. This is true for the hydrodynamics. Most literature focus on scaling to ensure the correct impact pressure [2], but this is of less importance here and the assumption of incompressible

flow is assumed to be good enough.

Froude scaling is applied by requiring the same Froude number in model and full scale. It is defined as

$$Fr = \frac{U}{\sqrt{gL}}, \tag{18}$$

where U and L are characteristic velocity and length respectively, while g is the gravity acceleration. Taking the velocity as the tank length divided by the sloshing period, T the criteria for scaling the motion period gets

$$T_m = T_f \sqrt{\lambda}, \tag{19}$$

and λ being the scale factor, $\lambda = L_m/L_f$. The subscripts m and f refer to model- and full scale respectively. Translational motion amplitude is scaled the same way, while angle amplitude is the same in model and full scale.

Scaling the motion like this may not be entirely correct without considering the Reynolds number. Although the fluid properties are quite different between natural gas and water, these differences are not within the scope to investigate.

What the thermodynamic response concerns, and condensation due to thermal mixing between liquid and gas, there are additional requirements for scaling. As the liquid subcooling is essential, while the gas superheating may be less important, the liquid *Jakob number* must remain the same. It is defined as the ratio of sensible to latent heat,

$$Ja = \frac{c_{v,L}\left(T_L - T_{sat}\right)}{h_{fg}}. \tag{20}$$

$c_{p,L}$ is the specific heat capacity and h_{fg} is the specific latent heat of formation. This requirement certainly involves fluid properties.

Another requirement is to ensure the same *thermo-mechanical* conditions. It may be enforced by considering an equation of state, like the ideal gas law, $P = \rho RT$. Scaling must satisfy:

$$\left(\frac{P}{\rho_G R T_G}\right)_f = \left(\frac{P}{\rho_G R T_G}\right)_m. \tag{21}$$

R is the gas constant and depends on the type of gas. If the gas is saturated, pressure and gas temperature are not both free variables. This would leave liquid bulk temperature, T_L and tank pressure, P as the only free variables.

LNG consist of 90 % methane. Comparing the properties of methane and water results in a linear relationship of ΔT and pressure. An example shows that a subcooling of $\Delta T_f = 6$ $[^\circ C]$ with liquid methane would need to be $\Delta T_m = 16$ $[^\circ C]$ with water. The influence of pressure is insignificant. If the same is done with Eq. 21, it is found that a pressure of 4-6 [barg] with methane would need to be as much as 15 [barg] with water. This condition is difficult to meet.

It is likely to believe that other factors matters than those mentioned here. For future studies, scaling should be investigated for these applications. This could be done by reducing the scale factor successively by increasing the tank size. Instead of comparing water and methane, the same considerations could be done with nitrogen and water to see if the scaling is satisfactorily. Improving the experimental facilities would be necessary. Another possibility to find the influence of fluid properties on sloshing is to run CFD simulations and systematically by changing viscosity and density.

7. Conclusion

The thermal response in a horizontal aligned pressure vessel of similar form as a marine LNG fuel tank was investigated by conducting experiments with a model scaled tank filled with water. Sloshing tests with a transparent tank has also been performed to study the the characteristic motion for different filling and frequencies. A theoretical analysis of the thermodynamics inside the tank was presented. The theory was implemented into a dynamic system model using the bond graph methodology. The model is based on tuning of parameters making a best fit of the results to extract information without performing steady-state calculations. The applicability of the model was investigated by estimating the PBU heat capacity. An estimate of the necessary heat capacity of the PBU from the measured pressure was presented. Scaling and similarity is discussed in the end of the paper.

The following conclusions can be made:

- Employing numerical integration to perform theoretical analysis is efficient and accurate. It provides the same information as steady-state calculations, but is less tedious.
- The mass flow rate of condensation and the pressure drop rate is proportional to the temperature difference between the saturation temperature and the liquid bulk temperature.
- The thermal equilibrium condition depends on the starting condition, while the pressure drop rate depends on the sloshing intensity. The sloshing intensity may be represented by the proposed parameter, $h_{iL} \cdot A_i$ which is nearly constant during the quasi-steady sloshing event.
- The time to reach the pressure minimum is the same time it takes to even out the temperature gradient on the liquid side.
- The time-instant heat required to maintain pressure was calculated numerically from the measured pressure. Time-averaged values are comparable to the measured ones, but this requires more investigation.
- The predicted heat needed to maintain pressure was significantly higher than the maximum PBU-power available. It is unlikely that an ordinary PBU has enough capacity to maintain pressure even in the case of less severe sloshing.
- Scaling of hydrodynamic motion and thermodynamic state may be considered separately if a two-way coupling due to compressible effects are neglected. Water as a substitute for methane is difficult in practice due to the different fluid properties.

Further work consist in improved formulation of the condensation mass flow rate. The definitions of the heat transfer coefficients must be changed to separate the heat transfer area. Including non-uniform temperature fields in the model would also improve the results. The effect of the heat transfer between fluid and walls should be investigated.

Acknowledgement

The authors would like to thank the staff at the Department of Maritime Technology and Operations for providing lab facilities and materials necessary to perform the experiments. This study is a part of a PhD project funded by NTNU in Ålesund.

References

[1] V. Æsøy, D. Stenersen, Low emission LNG fuelled ships for environmental friendly operations in arctic areas, in: ASME 2013 32nd International Conference on Ocean, Offshore and Arctic Engineering, American Society of Mechanical Engineers, 2013, pp. V006T07A028–V006T07A028.

[2] O. M. Faltinsen, A. N. Timokha, Sloshing, Cambridge University Press, 2009.

[3] E. Grotle, V. Æsøy, E. Pedersen, Modelling of LNG fuel systems for simulations of transient operations, Maritime-Port Technology and Development (2014) 205.

[4] E. W. Lemmon, M. L. Huber, M. O. McLinden, NIST Standard Reference Database 23: Reference Fluid Thermodynamic (2013). doi:http://dx.doi.org/10.18434/T4JS3C.
URL https://www.nist.gov/srd/refprop

[5] M. E. Moran, N. B. Mcnelis, M. T. Kudlac, M. S. Haberbusch, G. A. Satornino, Experimental results of hydrogen slosh in a 62 cubic foot (1750 liter) tank (1994).

[6] J. Lacapere, B. Vieille, B. Legrand, Experimental and numerical results of sloshing with cryogenic fluids, in: Progress in Propulsion Physics, Vol. 1, EDP Sciences, 2009, pp. 267–278.

[7] T. Arndt, Sloshing of Cryogenic Liquids in a Cylindrical Tank under normal Gravity Conditions, Universtität Bremen, 2011.

[8] C. Ludwig, M. Dreyer, E. Hopfinger, Pressure variations in a cryogenic liquid storage tank subjected to periodic excitations, International Journal of Heat and Mass Transfer 66 (2013) 223–234.

[9] E. L. Grotle, K. H. Halse, E. Pedersen, Y. Li, Non-isothermal sloshing in marine liquefied natural gas fuel tanks, in: The 26th International Ocean and Polar Engineering Conference, International Society of Offshore and Polar Engineers, 2016.

[10] S. M. Ghiaasiaan, Two-phase flow, boiling, and condensation: in conventional and miniature systems, Cambridge University Press, 2007.

[11] F. Kreith, R. F. Boehm, Direct-contact heat transfer, Springer Science & Business Media, 2013.

[12] S. Sideman, D. Moalem-Maron, Direct contact condensation, Advances in Heat Transfer 15 (1982) 227–281.

[13] H. B. Mahood, R. B. Thorpe, A. N. Campbell, A. O. Sharif, Experimental measurements and theoretical prediction for the transient characteristic of a two-phase two-component direct contact condenser, Applied Thermal Engineering 87 (2015) 161–174.

[14] J. Joseph, G. Agrawal, D. K. Agarwal, J. Pisharady, S. S. Kumar, Effect of insulation thickness on pressure evolution and thermal stratification in a cryogenic tank, Applied Thermal Engineering 111 (2017) 1629–1639.

[15] D. Karnopp, State variables and pseudo bond graphs for compressible thermofluid systems, Journal of Dynamic Systems, Measurement, and Control 101 (3) (1979) 201–204.

[16] P. O. Moksnes, Modeling two-phase thermo-fluid systems using bond graph, Dr. ing thesis, University of Sciences and Technology, Department of Marine Engineering, Norway.

[17] E. Pedersen, Modelling multicomponent two-phase thermodynamic systems using pseudo-bond graphs, SIMULATION SERIES 33 (1) (2001) 257–263.

[18] J. Thoma, B. O. Bouamama, Modelling and simulation in thermal and chemical engineering: A bond graph approach, Springer Science & Business Media, 2013.

[19] M. Moran, H. Shapiro, Fundamentals of Engineering Thermodynamics, Wiley, 2004.

[20] Controllab Products, 20-sim, `http://www.20sim.com`, [Online; accessed 31-January-2017] (2017).

[21] R. Bass, E. Bowles, R. Trudell, J. Navickas, J. Peck, N. Yoshimura, S. Endo, B. Pots, Modeling criteria for scaled lng sloshing experiments, Journal of Fluids Engineering 107 (2) (1985) 272–280.